Energy-dependent angular distribution of individual γ rays in the ^{139}La$(n,\gamma)^{140}$La* reaction

T. Okudaira,[1] S. Endo,[1,2] H. Fujioka,[3] K. Hirota,[1] K. Ishizaki,[1] A. Kimura,[2] M. Kitaguchi,[1] J. Koga,[4] Y. Niinomi,[1] K. Sakai,[2] T. Shima,[5] H. M. Shimizu,[1] S. Takada,[4] Y. Tani,[3] T. Yamamoto,[1] H. Yoshikawa,[5] and T. Yoshioka[4]

[1]*Nagoya University, Furocho, Chikusa, Nagoya 464-8602, Japan*
[2]*Japan Atomic Energy Agency, 2-4 Shirakata, Tokai, Naka, Ibaraki 319-1195, Japan*
[3]*Tokyo Institute of Technology, 2-12-1 Ookayama, Meguro, Tokyo 152-8551, Japan*
[4]*Kyushu University, 744 Motooka, Nishi, Fukuoka 819-0395, Japan*
[5]*Osaka University, 10-1 Mihogaoka, Ibaraki, Osaka 567-0047, Japan*

(Received 1 January 2021; accepted 20 May 2021; published 1 July 2021)

Neutron energy-dependent angular distributions were observed for individual γ rays from the 0.74 eV p-wave resonance of ^{139}La $+n$ to several lower excited states of ^{140}La. The γ-ray signals were analyzed in a two-dimensional histogram of the γ-ray energy, measured with distributed germanium detectors, and neutron energy, determined with the time-of-flight of pulsed neutrons, to identify the neutron energy dependence of the angular distribution for each individual γ rays. The angular distribution was also found for a photopeak accompanied with a faint p-wave resonance component. Our results can be interpreted as interference between s- and p-wave amplitudes, which may be used to study discrete symmetries of fundamental interactions.

DOI: 10.1103/PhysRevC.104.014601

I. INTRODUCTION

In the neutron absorption reaction of ^{139}La, extremely large parity violation with a size of $(9.56 \pm 0.35)\%$ was observed in the 0.74 eV p-wave resonance located on a tail of an s-wave resonance [1]. It is understood that fundamental parity violation in the nucleon-nucleon interaction of the order of 10^{-7} [2–4] is enhanced by the interference between s- and p-wave amplitudes, referred to as s-p mixing model [5,6]. The interference introduces a neutron energy-dependent angular distribution of γ rays in the vicinity of a p-wave resonance with respect to the incident neutron momentum [7]. Therefore, the angular distribution of γ rays provides important information to understand the enhancement mechanism of the parity violation in compound nuclei.

The neutron energy dependence of the angular distribution for individual γ rays was previously measured using a germanium detector assembly and the intense neutron beam at the Japan Proton Accelerator Research Complex (J-PARC) [8]. A clear angular distribution depending on the incident neutron energy was found in the vicinity of the p-wave resonance for the γ rays resulting from the transition of the 0.74 eV p-wave resonance of ^{139}La $+n$ to the ground state of ^{140}La.

In this paper, the angular distributions of the γ rays resulting from the 0.74 eV p-wave resonance to lower excited states of ^{140}La are studied as a function of the incident neutron energy by applying the same analysis method as in Ref. [8] to photopeaks for transitions to the lower excited states.

II. EXPERIMENT

A. Experimental setup

The data set used in this paper is the same as that used to evaluate the angular distribution of γ rays to the ground state. The measurement of the angular distribution of the individual γ rays in the ^{139}La$(n,\gamma)^{140}$La reaction was conducted using an intense pulsed neutron beam and a germanium detector assembly at beamline 04 of the Materials and Life Science Experimental Facility (MLF) at J-PARC [9]. The germanium detector assembly consists of 22 high-quality germanium crystals, pointing at angles from 36° to 144° with respect to the incident neutron beam direction [10]. A natural-abundant lanthanum metal plate with dimensions of 1 mm × 40 mm × 40 mm was placed at the detector center. The distance from the moderator surface to the La target is 21.5 m. The proton beam power was 150 kW and measurement time was 60 hours. A more detailed description of the experiment is given in Ref. [8].

B. MEASUREMENT

The same variables defined in Ref. [8] are used to evaluate the angular distributions of the γ rays in this paper. The deposit energy of the γ rays in the germanium crystal E_γ^{m} is obtained from the pulse height. The detection time of the γ rays t^{m} is measured from the timing pulse of the injection of the proton beam bunch. These are obtained for each γ-ray event. The variable t^{m} corresponds to the time of flight (TOF) of the incident neutrons for prompt γ rays, and the corresponding neutron energy E_n^{m} is calculated using t^{m}. The neutron energy in the center-of-mass system E_n is defined as well. The total number of γ-ray events detected in the experiment are denoted as I_γ. A two-dimensional histogram corresponding to $\partial^2 I_\gamma/\partial t^{\mathrm{m}}\partial E_\gamma^{\mathrm{m}}$ was obtained for each germanium crystal as the experimental result. The histogram of $\partial I_\gamma/\partial t^{\mathrm{m}}$ is shown in Fig. 1. The γ-ray events are integrated for $E_\gamma^{\mathrm{m}} \geqslant 2$ MeV to remove delayed γ rays. It is normalized

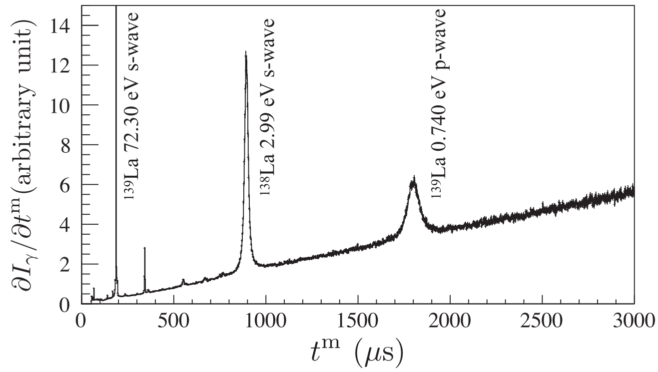

FIG. 1. γ-ray counts as a function of t^{m}. It is normalized relative to the incident beam intensity as a function of t^{m}.

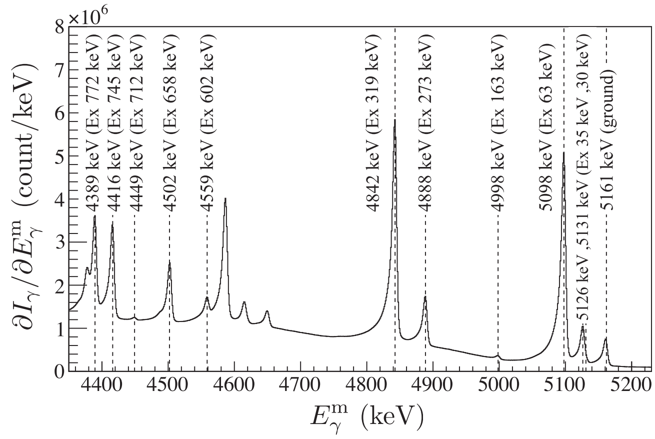

FIG. 2. Expanded γ-ray spectrum defined as $\partial I_\gamma/\partial E_\gamma^{\mathrm{m}}$. The dotted line shows the literature value of the photopeak energy. Three photopeaks around 4600 keV are single escape peaks from the γ rays of 5161 keV, 5131 keV, 5126 keV, and 5098 keV.

relative to the incident beam spectrum for t^{m}, which is obtained from a measurement of the 477.6 keV γ rays in the neutron absorption reaction of ^{10}B with an enriched ^{10}B target. The small peak at $t^{\mathrm{m}} \sim 1800\ \mu$s is the p-wave resonance, and the $1/v$ component is mainly derived from the tail of an s-wave resonance in the negative energy region as listed in Table I. Figure 2 shows a γ-ray spectrum defined as $\partial I_\gamma/\partial E_\gamma^{\mathrm{m}}$. Photopeaks of γ-ray transitions of ^{139}La$(n,\gamma)^{140}$La reactions to the lower excited and ground states are observed in Fig. 2. A schematic diagram of the level scheme of the ^{139}La$(n,\gamma)^{140}$La reaction is also shown in Fig. 3 [15]. Here, we focus on the intense transitions to the lower excited states of 30 keV, 35 keV, 63 keV, 273 keV, 319 keV, 658 keV, 745 keV, 772 keV, and the inclusive γ-ray transitions. Histograms of $\partial I_\gamma/\partial E_n^{\mathrm{m}}$ gated with each photopeak and inclusive γ rays are shown in Fig. 4. We can see that the 0.74 eV p-wave resonance appears in several transitions. Note that the histograms are the sum of all detector angles. The photopeak region was taken as the full width at the quarter maximum. Since the photopeaks of the 5126 keV and 5131 keV completely overlap, they are considered to be one photopeak. As a gated energy region for inclusive γ rays, 2000 keV $\leqslant E_\gamma^{\mathrm{m}} \leqslant$ 5170 keV was taken. The histograms were normalized by the incident neutron beam spectrum measured with the boron target. The background caused by the Compton-scattered γ rays for each photopeak was estimated by a third-order polynomial fit in the low- and high-energy region of each photopeak for each detector and subtracted. Since a loss of 2% of the total γ-ray counts occurred due to the DAQ system, a loss correction was also applied [8].

TABLE I. Resonance parameters of the neutron resonances of ^{139}La $+n$. The resonance parameters E_r, J_r, l_r, Γ_r^γ, g_r, and Γ_r^n are resonance energy, total angular momentum, orbital angular momentum, γ width, g factor, and neutron width, respectively. Parameter r denotes the resonance number. The spin and parity of ^{139}La are $7/2^+$, and therefore the p-wave resonance has negative parity.

r	E_r [eV]	J_r	l_r	Γ_r^γ [meV]	$g_r\Gamma_r^{\mathrm{n}}$ [meV]
1	-48.63[a]	4[a]	0	62.2[a]	(571.8)[a,*]
2	0.740 ± 0.002[b]	4[b]	1	40.41 ± 0.76[b]	$(5.6 \pm 0.5) \times 10^{-5}$[c]
3	72.30 ± 0.05[c]	3[b]	0	75.64 ± 2.21[d]	11.76 ± 0.53[d]

[a]References [11,12].
[b]Reference [8].
[c]Reference [13].
[d]calculated from References [14] and [13].
[*]The neutron width for the negative resonance was calculated using $|E_1|$ instead of E_1.

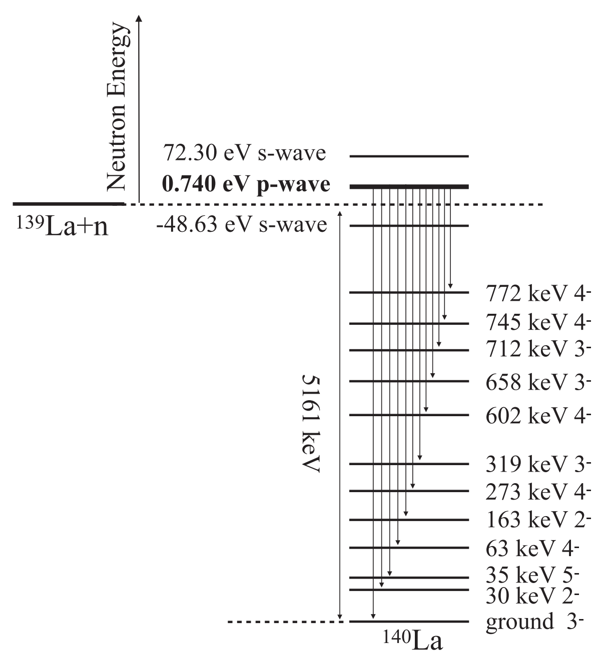

FIG. 3. Transitions from ^{139}La $+n$ to ^{140}La. The dashed line shows separation energy of ^{139}La $+n$. The transitions can actually occur not only from the p-wave resonance, but also from the s-wave resonances.

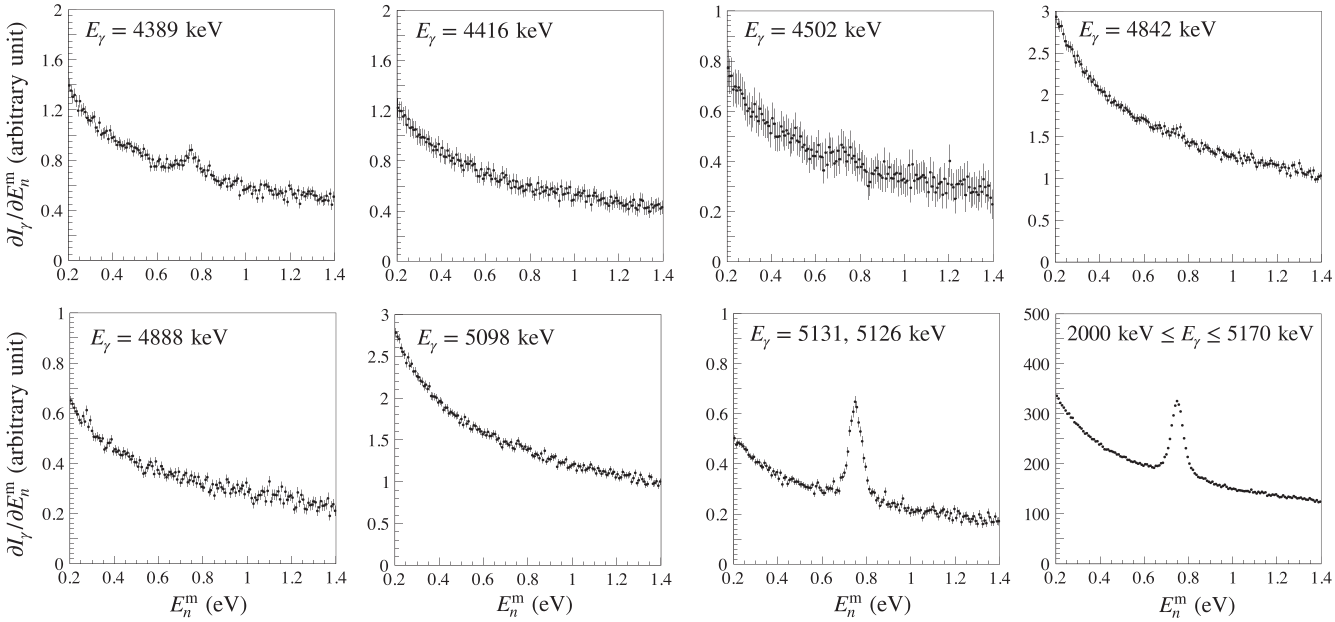

FIG. 4. γ-ray counts as a function of E_n^{m} gated with each photopeak and inclusive γ rays. The energy of photopeaks or the gated region of γ-ray energy show at the top left of each histogram.

C. Angular distribution

The neutron-energy dependence of the angular distribution causes an asymmetric resonance shape as a function of E_n^{m}, which is measured by a "low-high asymmetry" defined as

$$A_{\mathrm{LH}}(\theta_d) = \frac{N_{\mathrm{L}}(\theta_d) - N_{\mathrm{H}}(\theta_d)}{N_{\mathrm{L}}(\theta_d) + N_{\mathrm{H}}(\theta_d)}, \tag{1}$$

where θ_d is the detector angle with respect to the incident neutron momentum, and N_{L} and N_{H} are integrals in the region of $E_2 - 2\Gamma_2 \leqslant E_n \leqslant E_2$ and $E_2 \leqslant E_n \leqslant E_2 + 2\Gamma_2$, respectively. Variables E_2 and Γ_2 denote the resonance energy and total width of the p-wave resonance, which is defined by the γ width and neutron width shown in Table I as $\Gamma_2 = \Gamma_2^\gamma + \Gamma_2^n$. The definitions of N_{L} and N_{H} are shown in Eq. (8) in Ref [8] and Fig. 14 in Ref [8]. The low-high asymmetry is plotted for effective detector angle $\bar{\theta}_d$, which is obtained with a simulation of the germanium detector assembly [16], and fitted using a function of the form $A_{\mathrm{LH}}(\bar{\theta}_d) = A\cos\bar{\theta}_d + B$ with free parameters A and B. The angular distributions of A_{LH} for the photopeaks and inclusive γ rays are shown in Fig. 5. The fit results of A, which correspond to the angular distribution of the

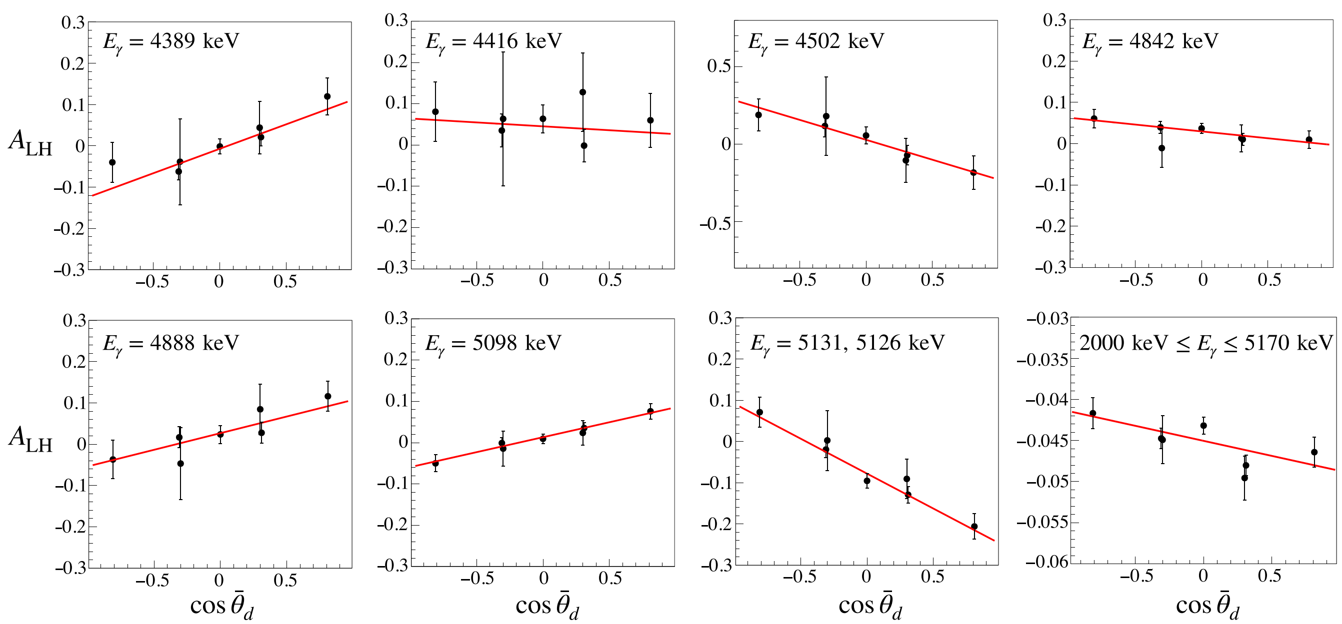

FIG. 5. Angular distributions of A_{LH} for each photopeak and inclusive γ rays. The solid lines are the fit results.

TABLE II. The fit results of A for each photopeak and inclusive γ rays.

E_γ [keV]	$E_{\rm ex}$ [keV]	F	A
4389	772	4, 5, 6	0.118 ± 0.030
4416	745	4	-0.020 ± 0.049
4502	658	3	-0.257 ± 0.078
4842	319	3	-0.033 ± 0.016
4888	273	4	0.081 ± 0.030
5098	63	4	0.072 ± 0.015
5131, 5126	30, 35	2,5	-0.169 ± 0.020
5161	0	3	-0.388 ± 0.024 [8]
inclusive			-0.0037 ± 0.0014

low-high asymmetry, are listed with the photopeak energy E_γ, excitation energy $E_{\rm ex}$, and the angular momentum of the final state F in the Table II. Nonzero angular distributions were found in the transition to the excited state of 30 keV and/or 35 keV, 63 keV, 658 keV, and 772 keV with a confidence level of over 99.7%.

III. DISCUSSION

A. Photopeak at 5098 keV

Although the p-wave resonance does not appear in the histogram of $\partial I_\gamma/\partial E_n^{\rm m}$ gated with 5098 keV photopeak as shown in Fig. 4, the angular distribution A is observed with a confidence level of over 99.7%. This phenomenon can also be confirmed using histograms of $\partial I_\gamma/\partial E_n^{\rm m}$ for 36° and 144° detectors shown in Fig. 6. In Fig. 6, the s-wave component, which obeys the $1/v$ law, is fitted using $f(E_n^{\rm m}) = a/\sqrt{E_n^{\rm m}} + b$ with free parameters a and b for the regions except for the p-wave resonance, and histograms before and after the subtraction of the s-wave component are shown. We can see that they have a slight asymmetric shape at 0.74 eV, and moreover, the shapes reverse with respect to 0.74 eV for 36° and 144° detectors. This angular-dependent asymmetric component has also been observed for 5161 keV photopeak as shown in Fig. 13 in Ref. [8] and is attributed to the interference term between s- and p-wave amplitudes. The significant value of

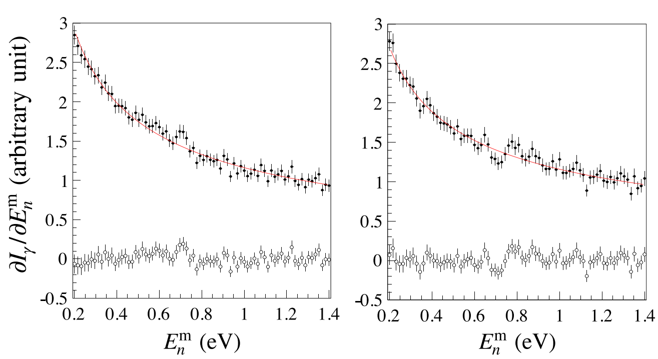

FIG. 6. γ-ray counts as a function of $E_n^{\rm m}$ gated with the 5098 keV photopeak for 36° (left) and 144° detectors (right). Solid lines show fit results to the s-wave component. Black points and white points show γ-ray counts before and after subtraction of the s-wave component, respectively.

A observed for faint γ-ray transition from the p-wave resonance can be understood as the result of the moderately weak transition amplitude of γ rays via the p-wave component; the magnitude of A is proportional to the product of the transition amplitudes of s- and p-wave components while the γ-ray intensity is proportional to the square of that of p-wave component. This interpretation is clarified by the differential cross section of (n, γ) reactions based on the s-p mixing model described in Appendix E in Ref. [8]. The ordinary p-wave resonance shown in Fig. 4 corresponds to the second term of a_0 in Eq. (E7) in Ref. [8], which has no angular distribution. In contrast, a_1, which is the interference term between s- and p-wave amplitudes, produces the angular-dependent asymmetric shape at the p-wave resonance for the detector angle satisfying $\cos\theta_\gamma \neq 0$ as shown in Eqs. (E1) and (E7) in Ref. [8]. The a_1 term in Eq. (E7) in Ref. [8] is proportional to the branching ratio from the p-wave resonance to the fth γ-ray transition λ_{2f}, whereas the second term of a_0 is proportional to λ_{2f}^2. Consequently, the second term of a_0 can be suppressed compared to a_1 when the branching ration from the p-wave resonance to the particular final state is small. In this way, the phenomenon that the 5098 keV photopeak has the angular distribution while no p-wave resonance appears can be explained by the interference term a_1 and the suppression of the a_0 amplitude due to the branching ratio.

B. Significance of the angular distribution

In order to confirm that the angular distributions are observed at the p-wave resonance, the angular distributions of $A_{\rm LH}$ were obtained for other neutron energies, not only within the vicinity of the p-wave resonance. The low-high asymmetry $A_{\rm LH}$ is calculated using $N_{\rm L}$ and $N_{\rm H}$ with the integral regions of $E_{\rm c} - 2\Gamma_2 \leqslant E_n \leqslant E_{\rm c}$ and $E_{\rm c} \leqslant E_n \leqslant E_{\rm c} + 2\Gamma_2$, respectively, where the center energy of the integral $E_{\rm c}$ takes a value of every 20 meV from 0 eV to 2 eV, and then the angular dependence A was obtained for every integral region. In Fig. 7, the significance of A is measured by a P-value, defined as $p = (1 - {\rm C.L.})/2$, where C.L. is the confidence level of the nonzero angular dependence. The P-value indicates the probability to observe a nonzero value of A in the hypothesis of no angular distributions. A confidence level of over 99.7% corresponds to a P-value less than 1.35×10^{-3}. As shown in the graph for $E_\gamma = 4389$ keV, 4502 keV, 5098 keV, and 5126 keV and/or 5131 keV in Fig. 7, significant angular distributions are observed only within the vicinity of the p-wave resonance.

This analysis suggests that the angular distribution measurement in the (n, γ) reaction is sensitive to search for faint γ-ray transitions from p-wave resonances.

IV. CONCLUSIONS

We observed significant angular distributions depending on the neutron energy for the γ rays in the transitions from the p-wave resonance of ^{139}La $+n$ to the several lower excited states of ^{140}La, including faint γ-ray transition from the p-wave resonance. This angular distribution can be interpreted as a result of the interference between s- and p-wave amplitudes. Recently, a transverse asymmetry has been measured for

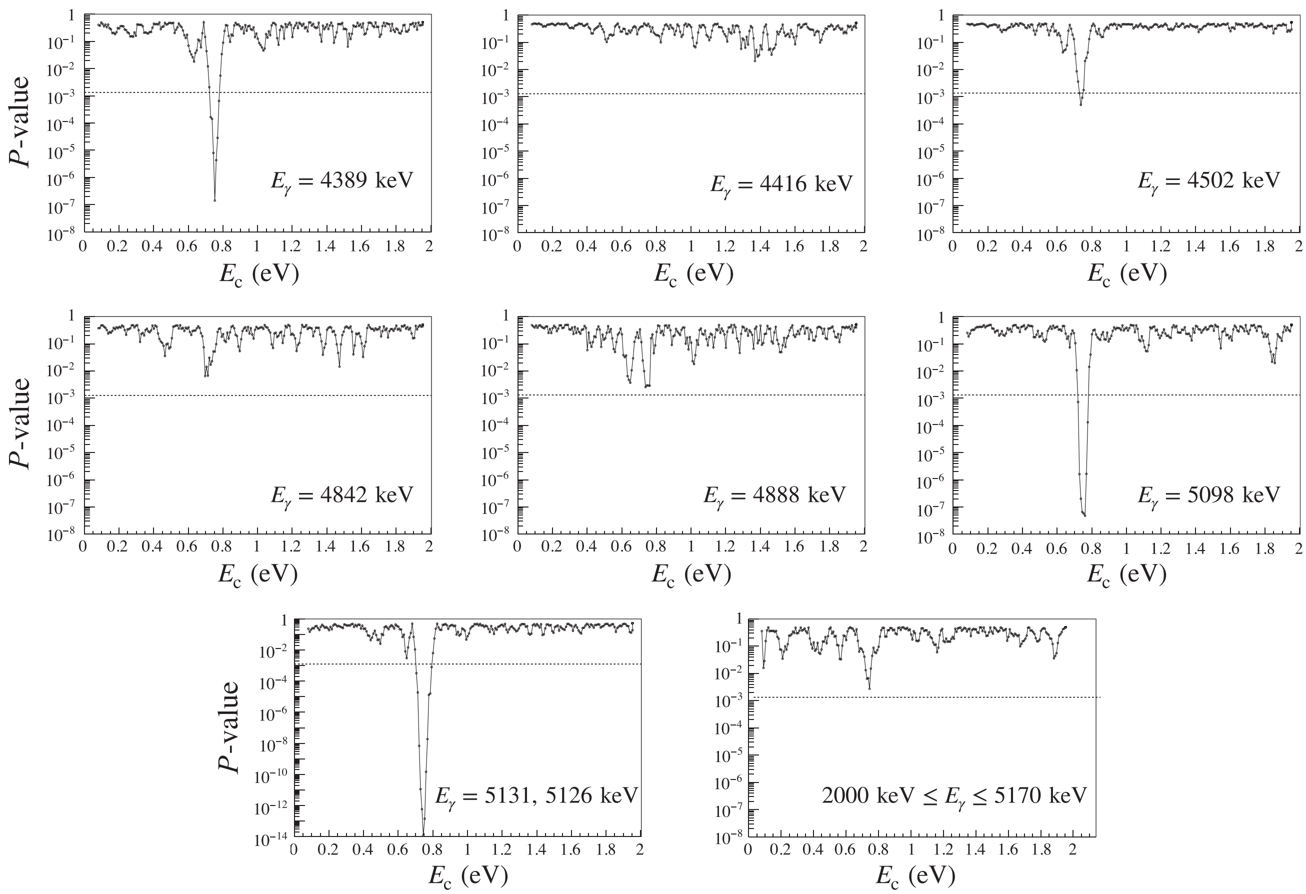

FIG. 7. P-values of the angular distribution of A_{LH} as a function of the center energy of the integral. The dotted lines show the P-value corresponding to the confidence level of 99.7%.

the p-wave resonance in the ^{139}La$(n, \gamma)^{140}$La reaction by using polarized epithermal neutrons [17], and these measurement results will be combined in terms of the s-p mixing model in order to understand the reaction mechanism of the enhancement of the symmetry violation to be published in a separate paper.

ACKNOWLEDGMENTS

The authors would like to thank the staff of beamline04 for the maintenance of the germanium detectors, and MLF and J-PARC for operating the accelerators and the neutron production target. The neutron scattering experiment was approved by the Neutron Scattering Program Advisory Committee of IMSS and KEK (Proposals No. 2014S03 and No. 2015S12). The neutron experiment at the Materials and Life Science Experimental Facility of the J-PARC was performed under a user program (Proposals No. 2016B0200, No. 2016B0202, No. 2017A0158, No. 2017A0170, No. 2017A0203). This work was supported by MEXT KAKENHI Grant No. JP19GS0210, JSPS KAKENHI Grants No. 17H02889, No. 19K21047, and No. 20K14495.

[1] V. P. Alfimenkov, S. B. Borzakov, V. V. Thuan, Y. D. Mareev, L. B. Pikelner, A. S. Khrykin, and E. I. Sharapov, Nucl. Phys. A **398**, 93 (1983).
[2] J. M. Potter, J. D. Bowman, C. F. Hwang, J. L. McKibben, R. E. Mischke, D. E. Nagle, P. G. Debrunner, H. Frauenfelder, and L. B. Sorensen, Phys. Rev. Lett. **33**, 1307 (1974).
[3] V. Yuan, H. Frauenfelder, R. W. Harper, J. D. Bowman, R. Carlini, D. W. MacArthur, R. E. Mischke, D. E. Nagle, R. L. Talaga, and A. B. McDonald, Phys. Rev. Lett. **57**, 1680 (1986).
[4] E. G. Adelberger and W. C. Haxton, Ann. Rev. Nucl. Part. Sci. **35**, 501 (1985).
[5] O. P. Sushkov and V. V. Flambaum, Usp. Fiz. Nauk **136**, 3 (1982).
[6] O. P. Sushkov and V. V. Flambaum, Sov. Phys. Usp. **25**, 1 (1982).
[7] V. V. Flambaum and O. P. Sushkov, Nucl. Phys. A **435**, 352 (1985).
[8] T. Okudaira, S. Takada, K. Hirota, A. Kimura, M. Kitaguchi, J. Koga, K. Nagamoto, T. Nakao, A. Okada, K. Sakai, H. M. Shimizu, T. Yamamoto, and T. Yoshioka, Phys. Rev. C **97**, 034622 (2018).
[9] M. Igashira, Y. Kiyanagi, and M. Oshima, Nucl. Instrum. Meth. Phys. Res. A **600**, 332 (2009).

[10] A. Kimura, T. Fujii, S. Fukutani, K. Furutaka, S. Goko, K. Y. Hara, H. Harada, K. Hirose, J. Hori, M. Igashira, T. Kamiyama, T. Katabuchi, T. Kin, K. Kino, F. Kitatani, Y. Kiyanagi, M. Koizumi, M. Mizumoto, S. Nakamura, M. Ohta *et al.*, and J. Nucl. Sci. Tech. **49**, 708 (2012).

[11] S. F. Mughabghab, *Atlas of Neutron Resonances* 5th ed. (Elsevier, Amsterdam, 2006).

[12] K. Shibata, O. Iwamoto, T. Nakagawa, N. Iwamoto, A. Ichihara, S. Kunieda, S. Chiba, K. Furutaka, N. Otuka, T. Ohsawa, T. Murata, H. Matsunobu, A. Zukeran, S. Kamada, and J. Katakura, J. Nucl. Sci. Technol **48**, 1 (2011).

[13] R. Terlizzi *et al.* (n_TOF Collaboration), Phys. Rev. C **75**, 035807 (2007).

[14] G. Hacken, J. Rainwater, H. I. Liou, and U. N. Singh, Phys. Rev. C **13**, 1884 (1976).

[15] N. Nica, Nucl. Data Sheets **108**, 1287 (2007).

[16] S. Takada, T. Okudaira, F. Goto, K. Hirota, A. Kimura, M. Kitaguchi, J. Koga, T. Nakao, K. Sakai, H. M. Shimizu, T. Yamamoto, and T. Yoshioka, J. Instrum. **13**, P02018 (2018).

[17] T. Yamamoto, T. Okudaira, S. Endo, H. Fujioka, K. Hirota, T. Ino, K. Ishizaki, A. Kimura, M. Kitaguchi, J. Koga, S. Makise, Y. Niinomi, T. Oku, K. Sakai, T. Shima, H. M. Shimizu, S. Takada, Y. Tani, H. Yoshikawa, and T. Yoshioka, Phys. Rev. C **101**, 064624 (2020).